JOURNAL OF THE ROYAL SOCIETY Interface

J. R. Soc. Interface (2009) **6**, 539–548
doi:10.1098/rsif.2008.0323
Published online 23 September 2008

Effect of Reynolds number and flow division on patterns of haemodynamic wall shear stress near branch points in the descending thoracic aorta

A. Kazakidi[1,2], S. J. Sherwin[1,*] and P. D. Weinberg[2]

[1]*Department of Aeronautics, and* [2]*Department of Bioengineering, Imperial College London, London SW7 2AZ, UK*

Atherosclerotic lesions are non-uniformly distributed at arterial bends and branch sites, suggesting an important role for haemodynamic factors, particularly wall shear stress (WSS), in their development. The pattern of lesions at aortic branch sites depends on age and species. Using computational flow simulations in an idealized model of an intercostal artery emerging perpendicularly from the thoracic aorta, we studied the effects of Reynolds number and flow division under steady conditions. Patterns of flow and WSS were strikingly dependent on these haemodynamic parameters. With increasing Reynolds number, WSS, normalized by the fully developed aortic value, was lowered at the sides of the ostium and increased upstream and downstream of it. Increasing flow into the side branch exacerbated these patterns and gave rise to a reversing flow region downstream of the ostium. Incorporation of more realistic geometric features had only minor effects and patterns of mean WSS under pulsatile conditions were similar to the steady flow results. Aspects of the observed WSS patterns correlate with, and may explain, some but not all of the lesion patterns in human, rabbit and mouse aortas.

Keywords: haemodynamics; atherosclerosis; wall shear stress; arterial branches; aorta

1. INTRODUCTION

Atherosclerosis, the disease underlying most heart attacks and strokes, is characterized by the focal accumulation of lipid, cells and connective tissue components within the arterial wall. The non-uniform distribution of these lesions in areas of branching and curvature is consistent with a controlling influence of stresses imposed on the wall by the flow of blood. The current consensus is that lesions occur most frequently in regions of low and fluctuating haemodynamic wall shear stress (WSS). However, there are differences in the distribution of lesions between species, and between ages within a species, that challenge this consensus. Here we report an investigation of whether the pattern of WSS is sensitive to factors such as Reynolds number (Re) and flow division and hence could vary with species and age, or whether it is invariant, implying that the consensus may not apply to all the observed lesion distributions.

Differences in the distribution of lesions between species and ages have been most completely documented for the origins of intercostal arteries within the descending thoracic aorta (Weinberg 2002). In human foetuses, neonates and infants, fatty streaks occur around the downstream margins of these branch ostia (Sinzinger *et al.* 1980). At later ages, however, they occur at the lateral and then the upstream margins (Sloop *et al.* 1998), while advanced disease tends to completely surround the ostium (Mitchell & Schwartz 1965). Spontaneous and diet-induced lesions in immature and mature rabbits show the first two patterns (Barnes & Weinberg 1998, 1999) whereas lesions completely surround intercostal ostia regardless of age in knockout mice lacking the low-density lipoprotein receptor and apolipoprotein E (McGillicuddy *et al.* 2001).

Numerous previous studies using analytical techniques, physical models or computational methods have investigated patterns of flow or WSS in the vicinity of arterial branch points. More recently, allometric studies have examined variations in WSS between species, proposing various scaling laws (Greve *et al.* 2006; Cheng *et al.* 2007; Weinberg & Ethier 2007). However, only a few have systematically studied the effects on WSS of varying Re or flow division between parent and daughter vessel (Cheer *et al.* 1998) and we are not aware of any that have attempted to explain the age- and species-dependent differences in lesion pattern.

This study used high-order spectral/hp element methods (Karniadakis & Sherwin 2005) to compute flow fields and WSSs in the vicinity of model intercostal branch ostia using a range of these parameters.

*Author for correspondence (s.sherwin@imperial.ac.uk).

Received 27 July 2008
Accepted 4 September 2008

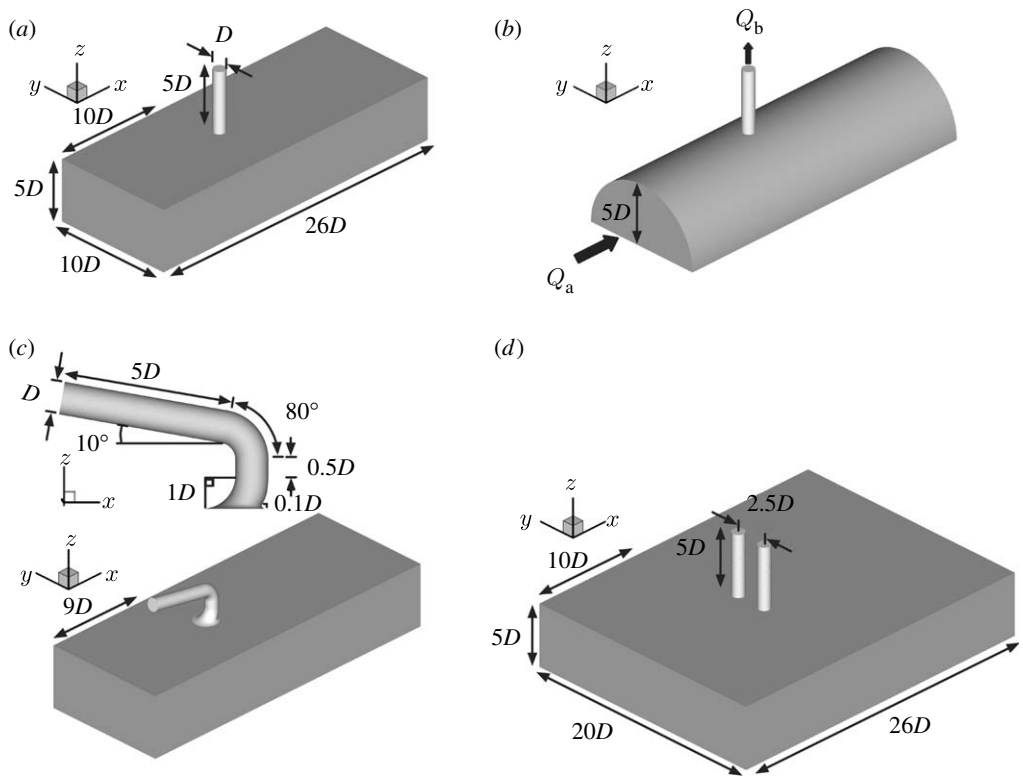

Figure 1. Computational domains representing intercostal arteries branching from the thoracic aorta: (*a*) simple model of one intercostal artery emerging perpendicularly from the thoracic aorta, (*b*) more realistic aortic geometry, (*c*) more realistic geometry of the aorto-intercostal junction, and (*d*) pair of branches at the same streamwise position. Dimensions in (*b*) and (*c*), other than those shown, are the same as in (*a*). The unit of length, D, is the diameter of the intercostal artery. The flow direction is shown in (*b*) and is the same for all models.

The range includes values appropriate for human subjects and for the smaller animals that are widely used as models of the human disease. For the majority of computations, a number of simplifying assumptions were made, most importantly that of steady flow, but the work nevertheless gives insight into the patterns of WSS to be expected *in vivo*, the flow fields that explain them, and the possibility that changes in these parameters might account for different patterns of disease.

2. METHODS

2.1. Geometry

In people, rabbits and mice, intercostal arteries originate from the dorsal surface of the descending thoracic aorta in pairs. Effects of varying Re and flow division were first examined on a single branch and subsequently on a pair of branches. For most computations, the geometry of the single branch was approximated as a cylindrical tube, representing the intercostal artery, emerging perpendicularly from a flat surface, representing the dorsal wall of the descending thoracic aorta (figure 1*a*); similar models of intercostal branches have previously been used by Sobey (1977*a*,*b*) and Tutty (1988). The assumption of a flat aortic wall is justified because the diameter of the intercostal artery (D_b) is substantially smaller than that of the thoracic aorta (D_a). Based on previous estimates (Sobey 1977*a*,*b*; Pedley 1980; Tutty 1988) and *in vivo* measurements (Cornhill & Roach 1976; Caro *et al.* 1978; Nichols & O'Rourke 1998), $D_b : D_a$ was assumed to equal 0.1.

Taking D_b (hereafter D) as the unit of length, a segment of aortic wall near the branch was approximated by a rectangular channel $26D$ long in the axial (x) direction, $10D$ wide in the crossflow (y) direction and $5D$ high in the z direction (figure 1*a*). The cylindrical tube representing the intercostal artery had length $5D$. It was located on the longitudinal centreline of the aortic wall segment and its upstream lip was $10D$ from the upstream edge of the aortic segment.

In studies to assess the sensitivity of the solution to geometric assumptions, the width of the aortic channel was doubled and the sharp edge of the aorto-intercostal junction was replaced with a rounded lip with radius of curvature $0.1D$. In a further study, the aorta was modelled as a half cylinder of $10D$ and the branch junction as the intersection of two perpendicular cylinders (figure 1*b*). Flow was also computed for a more realistic model (figure 1*c*) in which the inflow tract and flow divider had geometries approximating those seen in histological sections (e.g. Sebkhi & Weinberg 1994, 1996) and the side branch curved back towards the heart, as observed in corrosion casts (Abrahams 2001; B. A. Nier & P. D. Weinberg 2005, unpublished data). The aim was neither to reconstruct an actual branch nor to define an average geometry but to determine whether the patterns of WSS seen in the simpler model are likely also to apply to geometries of the broad type seen *in vivo*.

For the case of a pair of intercostal arteries, the width of the domain was again doubled to $20D$ and two cylindrical tubes of the radius and height used previously

were symmetrically situated about the longitudinal centreline with a centre-to-centre separation of $2.5D$ and were (i) both positioned with their upstream lips $10D$ from the upstream edge of the domain (figure 1*d*) or (ii) staggered in the axial direction, their upstream lips being $10D$ and $11D$ from the upstream edge. The separation approximates the minimum observed in en face images of rabbit aortas fixed *in situ* at physiological pressure (A. R. Bond 2005, personal communication). Both unstaggered and staggered geometries were used since stagger tends to increase with distance down the aorta. In all cases, walls were assumed to be rigid.

2.2. Governing equations and boundary conditions

The flow was assumed to be governed by the Newtonian incompressible Navier–Stokes equations

$$\rho\frac{\partial \boldsymbol{u}}{\partial t}+\rho(\boldsymbol{u}\cdot\nabla)\boldsymbol{u}=-\nabla p+\mu\nabla^2\boldsymbol{u},$$

$$\nabla\cdot\boldsymbol{u}=0,$$

where $\boldsymbol{u}=[u,v,w]$ is the velocity vector; ρ is the fluid density; p is the static pressure; and μ is the dynamic viscosity. The flow is characterized by the Reynolds number defined as $Re=\rho\bar{u}_\mathrm{a}D_\mathrm{a}/\mu$, where $\bar{u}_\mathrm{a}$ is the average velocity of the fluid in the aorta of diameter $D_\mathrm{a}=10D$.

Since the near branch region was approximated as a channel rather than a pipe, the velocity profile imposed at the upstream end of the computational domain was assumed to be parabolic in the z direction. Furthermore, as the computational domain was defined over only half the aortic diameter, i.e. $5D$, the peak of the parabolic velocity was imposed at the surface of the computational domain opposite to the aortic wall (the bottom plane of the computational domains shown in figure 1*a*,*c*,*d*). The only non-zero aortic inflow velocity component was therefore $u_\mathrm{a}=u_\mathrm{a}(z)$, which in non-dimensional form can be written (assuming $z=0$ is the channel centreline) as

$$\frac{u_\mathrm{a}}{\bar{u}_\mathrm{a}}(z)=\frac{3}{2}\left(1-\frac{z^2}{25D^2}\right).$$

For the geometry of figure 1*b*, the fully developed pipe flow condition was considered, which in non-dimensional form can be expressed as

$$\frac{u_\mathrm{a}^\mathrm{pipe}}{\bar{u}_\mathrm{a}^\mathrm{pipe}}(y,z)=2\left[1-\frac{(y-y_{\mathrm{a}0})^2}{25D^2}-\frac{z^2}{25D^2}\right],$$

where $y_{a0}=5D$.

The aortic flow rate, Q_a, was defined as

$$Q_\mathrm{a}=\bar{u}_\mathrm{a}A_\mathrm{a}=\bar{u}_\mathrm{a}100D^2,$$

where A_a is the full height channel inflow area $100D^2$. Clearly, if the aorta had been modelled as a pipe the cross-sectional area would have been $A_\mathrm{a}^\mathrm{pipe}=\pi D_\mathrm{a}^2/4\cong 0.8\times100D^2$ and so the equivalent pipe flow rate is 80 per cent of that considered in the following.

The outflow velocity, $w_\mathrm{b}(x,y)$, at the side branch (where $u_\mathrm{b}=v_\mathrm{b}=0$) can be written in non-dimensional form as

$$\frac{w_\mathrm{b}}{\bar{w}_\mathrm{b}}(x,y)=2\left[1-4\left(\frac{x-x_0}{D}\right)^2-4\left(\frac{y-y_0}{D}\right)^2\right],$$

where $\bar{w}_\mathrm{b}$ is the side branch average velocity; A_b is the branch cross-sectional area; and $x_0=10.5D$, $y_0=5D$. Finally, the side branch pipe flow rate, Q_b, is defined as

$$Q_\mathrm{b}=\bar{w}_\mathrm{b}A_\mathrm{b}=\bar{w}_\mathrm{b}\pi D^2/4.$$

2.3. Computational methods

Non-proprietary software was used to create a hybrid mesh of body-conforming prismatic and unstructured tetrahedral elements (Peiró *et al.* 2002; Sherwin & Peiró 2002). A prismatic boundary-layer mesh was used at the wall to enhance the modelling of viscous flows (Papaharilaou *et al.* 2002); in all cases, it had a thickness of $0.3D$. For the simple, single-branch geometry, a mesh of 452 prismatic and 2116 tetrahedral elements was generated. To test that this was sufficient, a mesh with 908 prismatic and 6536 tetrahedral elements was also created. The increase in the total number of mesh elements from 2568 to 7444 changed the streamwise force on the aortic wall by less than 0.01 per cent. The mesh for the more realistic geometry contained 25 391 elements (1950 prisms and 23 441 tetrahedra), while those for the staggered and unstaggered pairs of branches contained 13 446 (1668 prisms, 11 778 tetrahedra) and 13 523 (1664 prisms, 11 859 tetrahedra) elements, respectively. Finally, for the geometry of figure 1*b* a mesh of 7034 elements (902 prisms, 6132 tetrahedra) was used.

The solution was computed using a spectral/hp element method described by Karniadakis & Sherwin (2005). The code has previously been used in various applications (Sherwin *et al.* 2000; Giordana *et al.* 2005). An increase of the order of the polynomial expansion within each element from four to six produced an approximately 2 per cent decrease in the streamwise force. Hence, the computations were performed at a polynomial order of six, which for the main mesh of the simple geometry (figure 1*a*) corresponds to 266 336 local degrees of freedom per variable.

3. RESULTS

The main results of our study are summarized in figure 2, which shows aortic WSS magnitude around the ostium of the simple model for a range of Re and flow divisions ($Q_\mathrm{b}:Q_\mathrm{a}$). Surface streamlines indicating flow direction immediately above the wall are also shown. WSS was normalized by the inflow WSS (equivalent to the local shear rate relative to the inflow shear rate). Effects of holding $Q_\mathrm{b}:Q_\mathrm{a}$ at its lowest value and varying Re (figure 2*a*–*d*) are considered first, effects of varying $Q_\mathrm{b}:Q_\mathrm{a}$ at the lowest value of Re (figure 2*a*,*e*,*i*,*m*) are considered next, and lastly effects of changing Re and $Q_\mathrm{b}:Q_\mathrm{a}$ together are described.

3.1. Effect of Re at constant flow partition

Figure 2*a*–*d* shows results for $Q_\mathrm{b}:Q_\mathrm{a}$ held at 0.08 per cent. At $Re=30$, the lowest value examined, normalized WSS ($\mathrm{WSS_n}$) was comparatively uniform around the ostium, with only slightly elevated values on the ostial lip, and the surface streamlines were

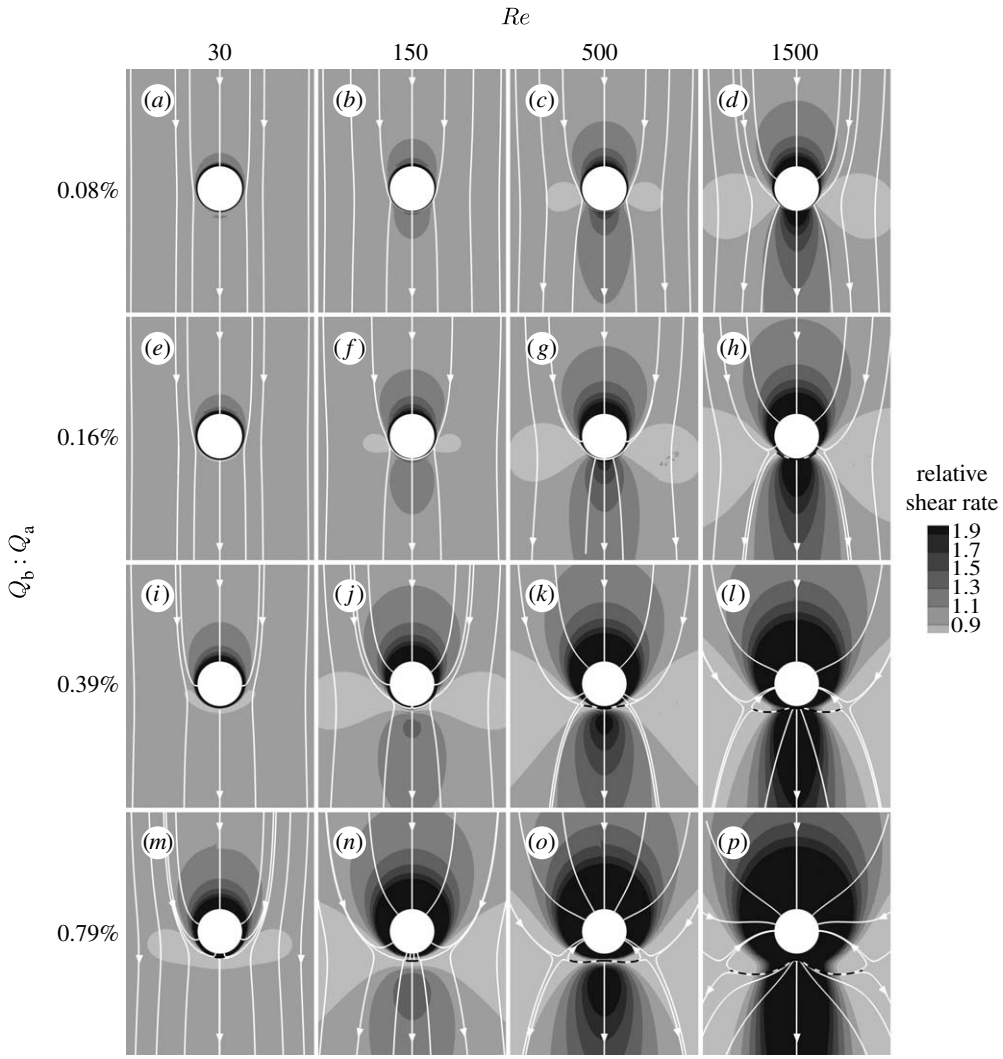

Figure 2. Magnitude and direction of non-dimensionalized aortic WSS around the ostium of the simple intercostal junction of figure 1*a*. (*a–p*) Mean aortic flow is from top to bottom. The simulations were performed at a range of *Re* and flow partitions to account for different species and ages within a species. Dashed lines indicate flow attachment.

everywhere almost parallel to the longitudinal axis. At $Re=150$, WSS_n was slightly elevated immediately upstream and downstream of the branch orifice and the upstream streamtraces converged towards the ostium. As *Re* was further increased to 500, the upstream and downstream regions of high WSS_n enlarged, the downstream region taking on the shape of a streak, and WSS_n decreased at the lateral margins of the orifice. These trends in WSS_n were exaggerated when *Re* was at its maximum of 1500. Streamlines in the upstream region converged more sharply towards the orifice (suggesting local acceleration of fluid particles) and diverged in the downstream region (suggesting local deceleration). In all cases, the streamlines were symmetrical about the centreline although this was not explicitly imposed by the numerical algorithm (see §4 and figures 5*a* and 6*a* for an analysis of the flow features underlying these patterns).

3.2. Effect of flow partition at constant Re

Figure 2*a*,*e*,*i*,*m* shows WSS_n patterns and surface streamlines calculated for $Re=30$. At the lowest side branch flow partition ($Q_b : Q_a=0.08\%$), WSS_n was almost uniform except for slightly increased values on the ostial lip, and the streamlines were almost straight, as noted above. As $Q_b : Q_a$ increased, a region of higher WSS_n developed upstream of the ostium, where the surface streamlines converged towards the branch, suggesting acceleration of the near-wall fluid. Increases in $Q_b : Q_a$ also reduced WSS_n in a circumscribed region immediately downstream of the branch, except on the lip itself where it remained elevated. Streamlines diverged in this area. (Effects of increasing flow partition on the flow field underlying these patterns are presented in §4 and figures 5*a* and 6*b*.)

3.3. Effects of changing Re and $Q_b : Q_a$ together

The remainder of figure 2 shows WSS_n patterns and surface streamlines for other combinations of these values of *Re* and $Q_b : Q_a$. In all rows, increasing *Re* led to a decrease of WSS_n at the sides of the branch and an increase upstream and downstream. In all columns, increasing $Q_b : Q_a$ enlarged the areas where WSS_n was altered and intensified the differences in its magnitude. It also moved the low-shear side lobes downstream and extended the downstream region of reversed flow. In every case, the upstream region was characterized by

elevated WSS_n; this region extended further upstream and around the orifice at higher Re and $Q_b : Q_a$. At these higher values, attachment lines were observed downstream of the branch ostium, and they enlarged with increasing Re and $Q_b : Q_a$.

3.4. WSS_n at paired intercostal branches

The two configurations for paired branches—ostia at the same and at staggered streamwise positions—were tested at $Re=500$ and $Q_b : Q_a=0.79$ per cent. In both cases (figure 3), the pattern of WSS_n around each ostium was broadly similar to that observed for a single branch under the same conditions (figure 2*o*). Differences were restricted to the region between the two ostia, where the areas of low WSS_n seen to the sides and slightly downstream of individual ostia were truncated and merged. The WSS_n pattern was symmetrical about the axial midline when the ostia were at the same streamwise position, but not when they were staggered. Interestingly, no fluid flowing close to the wall between the two ostia appeared able to move downstream of the ostia; rather, the flow turned towards one or other of them. In the staggered case, there was a more complex pattern that maintained many of the topological features of the unstaggered case. However, the downstream centreline stagnation point in the unstaggered case split into two stagnation points in the staggered configuration.

3.5. Effects of geometric assumptions

To test the possibility that the side boundary conditions affected the results, WSS_n and surface streamlines were examined after the aortic channel had been doubled in width. At $Re=500$ and $Q_b : Q_a=0.79$ per cent, there was an approximately 3 per cent increase in the mean WSS in a square region of size $3D$ centred around the branch ostium.

The effect of rounding the sharp edges of the aorto-intercostal junction was also investigated at $Re=500$ and $Q_b : Q_a=0.79$ per cent. There was an approximately 1.7 per cent decrease in the streamwise-acting force.

Modelling the aorta as a half cylinder (figure 1*b*), with the junction being the intersection between two perpendicular cylinders, did not qualitatively alter the pattern of WSS around the branch ostium at $Re=500$ and $Q_b : Q_a=0.79$ per cent (figure 4*a*). The high WSS_n region upstream and around the ostial lip was reduced slightly in magnitude.

Finally, using the more realistic geometry of figure 1*c*, again at $Re=500$ and $Q_b : Q_a=0.79$ per cent, the WSS_n pattern (figure 4*b*) appeared nearly identical in character to the equivalent obtained for the simple geometry. WSS_n remained elevated upstream of the ostium despite the gently curving inflow tract.

4. DISCUSSION

We used computational fluid dynamic techniques to examine the effect of Reynolds number, Re, and flow partition, $Q_b : Q_a$, on aortic WSS around the origins of intercostal arteries. The study was motivated by the observation that the pattern of atherosclerosis, putatively a shear-dependent disease, varies between species and with age at this site. We wished to determine whether patterns of WSS can also vary. The values of Re that we studied are appropriate for species ranging from mice to people (Buchanan *et al.* 1999; Shahcheraghi *et al.* 2002; Feintuch *et al.* 2007). Flow partitions have not been measured accurately at intercostal branch sites in any species. Furthermore, there is disagreement as to whether flow in general partitions according to the square or the cube of the ratio of vessel diameters (Cheng *et al.* 2007), which would correspond to $Q_b : Q_a=1$ per cent or 0.1 per cent, respectively, for the models examined in this study. Partitions will certainly vary with physiological demand and may also depend on species and age. We therefore investigated a wide range encompassing or closely approaching these values. Our main finding was that the pattern of WSS is highly dependent on Re and flow partition.

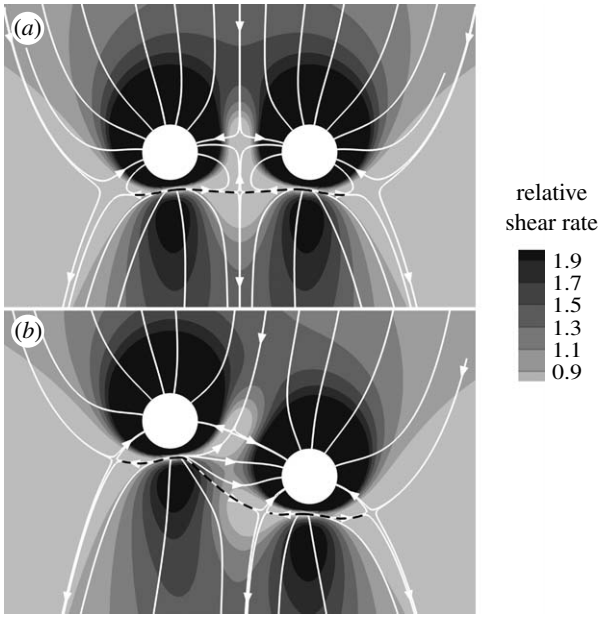

Figure 3. Magnitude and direction of non-dimensionalized aortic WSS around a pair of intercostal ostia at (*a*) the same streamwise position and (*b*) staggered positions. Mean aortic flow is from top to bottom. The simulations were performed for $Re=500$ and $Q_b : Q_a=0.79\%$. Dashed lines indicate flow attachment.

The fundamental features of the flow underlying the different patterns of WSS_n shown in figure 2 can be elucidated by computing streamlines along the mid-plane of the aortic channel (figure 5) and by computing streamtubes of fluid moving into the branch (figure 6). To obtain the streamtubes, a ring of fluid particles at a distance $2D$ down the branch and with diameter $0.8D$ was traced backwards into the aorta to examine its origins (Coppola *et al.* 2001). Figure 6 includes simulations at higher values of Re and $Q_b : Q_a$ than figure 2, to confirm the trend in their effects on the streamtube. Perspective views of the streamtube are shown in figure 6 (on the right).

These figures show that increasing Re causes fluid to enter the branch from regions closer to the aortic

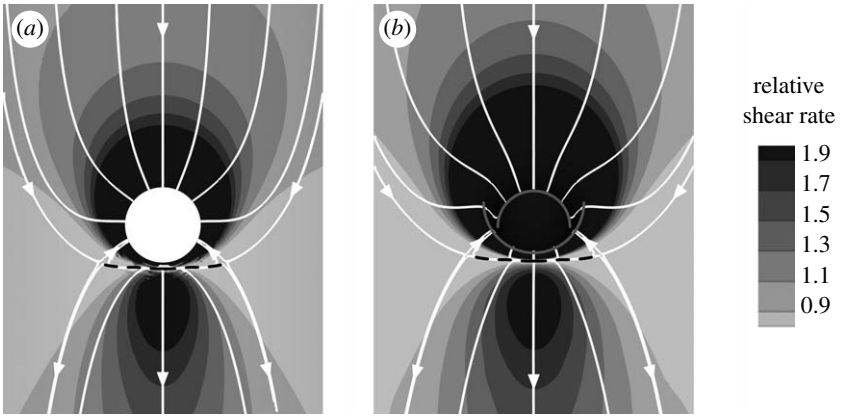

Figure 4. Magnitude and direction of non-dimensionalized aortic WSS around the ostium of (*a*) the aortic model of figure 1*b* and (*b*) the realistic aorto-intercostal junction of figure 1*c*. Mean aortic flow is from top to bottom. The simulations were performed for $Re=500$ and $Q_b : Q_a=0.79\%$. Dashed lines indicate flow attachment.

wall. For example, the streamline that divides the fluid entering the branch from that continuing down the aorta moves towards the aortic wall in figure 5*a* when Re is increased from 30 to 1500. At $Re=1500$, fluid flow in the mainstream has too much momentum to enter the branch; instead, fluid is drawn down the side branch from a wider area nearer the wall, where it is moving more slowly (figure 6*a*). This shift of the streamtube nearer to the wall leads to a greater influence of the branch on WSS around the ostium. The resulting divergence of surface streamlines lateral to the ostium (figure 2) leads to a reduction in WSS, as the flow slows down between them (providing that streamlines just above the surface remain parallel to the wall, as is the case). The inability of mainstream fluid to be drawn down the branch also provides an insight into why an attachment line develops downstream of the ostium at higher values of Re: a greater amount of slow moving, near-wall fluid is drawn down the branch, initially from lateral regions but then from downstream regions (figure 2*i–p*).

Increasing the flow partition $Q_b : Q_a$ necessarily increases the cross-sectional area of the streamtube in the aorta. These streamtubes remain similar in shape to the ones seen at lower $Q_b : Q_a$ (figure 6*b*), explaining why greater flow into the branch intensifies and enlarges some features of the WSS patterns (figure 2 *a*,*e*,*i*,*m*; *b*,*f*,*j*,*n*; *c*,*g*,*k*,*o*; *d*,*h*,*l*,*p*) but does not fundamentally alter the flow physics. However, at some value of $Q_b : Q_a$ the need for more fluid to enter the branch requires fluid to be drawn from downstream of the ostium and so the streamlines along the mid-plane can be seen to overshoot the branch mouth before entering the branch (figure 5*a*). This mechanism explains why the attachment line (and by analogy the lateral areas of low WSS_n) moves downstream as $Q_b : Q_a$ increases (figure 2*a*,*e*,*i*,*m*; *b*,*f*,*j*,*n*; *c*,*g*,*k*,*o*; *d*,*h*,*l*,*p*). This property can lead to a shift from an increase to a decrease in WSS_n in regions immediately downstream of the ostium. Finally, considering figure 2*a*,*e*,*i*,*m*; *b*,*f*,*j*,*n*; *c*,*g*,*k*,*o*; *d*,*h*,*l*,*p*, we observe that as $Q_b : Q_a$ increases there is a reduction of WSS_n lateral to the ostium. Again this correlates with a divergence of the surface streamlines. As noted above, this explanation assumes that streamlines above the surface remain parallel to the wall. In our data analysis, we observed some distortion of these streamlines with increasing $Q_b : Q_a$ but not to an extent that could compensate for the lateral divergence of the surface streamlines; hence the average flow in this region is reduced, leading to a reduction in WSS_n.

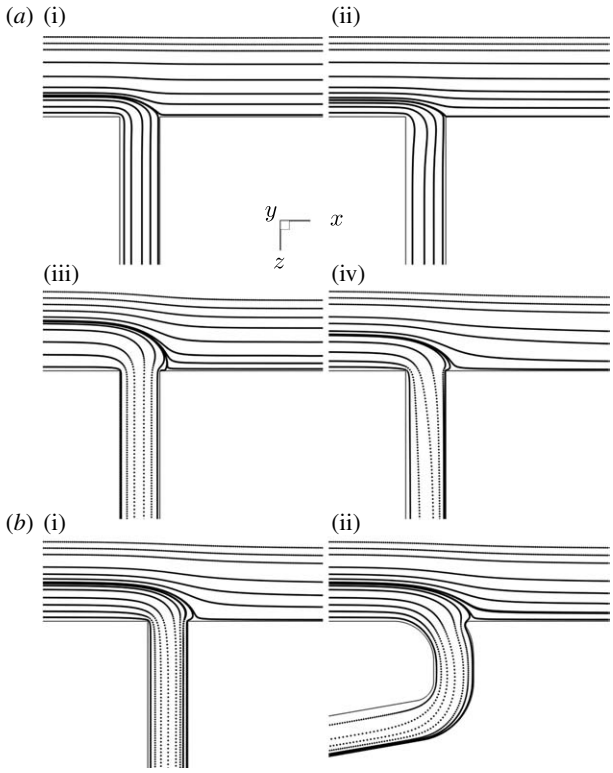

Figure 5. Streamlines along the mid-plane of the domain. (*a*) Streamlines for the simple model of figure 1*a*; (*a*(i)–(iv)) correspond to the four combinations ($Re=30$, 1500, 30, 1500, respectively, and $Q_b : Q_a=0.08$, 0.08, 0.79, 0.79%, respectively) of highest and lowest Re and $Q_b : Q_a$ in figure 2. (*b*) Streamlines in (i) the simple model and (ii) the more realistic model of figure 1*c* at $Re=500$ and $Q_b : Q_a=0.79\%$. Mean aortic flow is from left to right in all cases.

Figure 7 is a line graph showing the changes in WSS_n observed with increasing Re at $Q_b : Q_a=0.08$ per cent (figure 7*a*), and with increasing $Q_b : Q_a$ at $Re=30$ (figure 7*b*) in the simple geometry (figure 1*a*). Maps

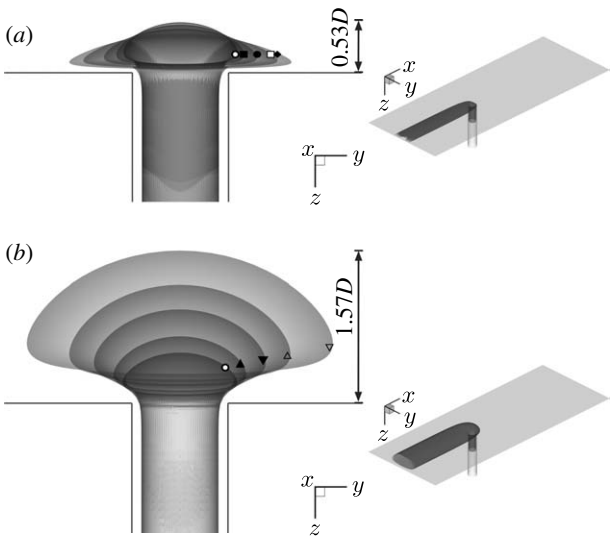

Figure 6. Computed streamtubes of fluid entering the branch. (*a*) Effect of increasing Re at $Q_b : Q_a = 0.08\%$ (Re: open circle, 30; filled square, 150; filled circle, 500; open square, 1500; filled diamond, 2500). (*b*) Effect of increasing $Q_b : Q_a$ at $Re = 30$ ($Q_b : Q_a$: open circle, 0.08%; filled uptriangle, 0.16%; filled downtriangle, 0.39%: open uptriangle, 0.79%; open downtriangle, 1.73%). Perspective views of the streamtubes are shown on the right.

of WSS_n contours shown for these conditions in figure 2*a–d* and *a*,*e*,*i*,*m*. In figure 7, WSS_n is instead shown more precisely for three locations on the aortic wall: one side branch diameter (D) upstream of the ostial lip, 1D downstream of it, and 1D lateral to it. (Figure 7 also includes simulations at higher values of Re and $Q_b : Q_a$ than in figure 2, to confirm the trend in their effects on the WSS_n.) At the lowest Re and $Q_b : Q_a$, WSS_n was almost uniform around the branch and had a magnitude close to the inflow normalized value of 1 at all three locations. WSS_n rose more rapidly downstream than upstream with increasing Re, but the opposite was seen with increasing $Q_b : Q_a$, where values in the downstream region rose only slightly before falling again. Increasing either Re or $Q_b : Q_a$ decreased WSS_n lateral to the lip, as explained above.

4.1. Simplifying assumptions

Re and $Q_b : Q_a$ were systematically varied in an idealization of the aorto-intercostal junction consisting of a cylindrical branch emerging from a flat plate. Using an idealized geometry can help elucidate underlying mechanisms that would be obscured or attributed to geometric features in a more complex model, but may also introduce artefacts or fail to replicate important facets of *in vivo* flows. The effects of the simplification were examined by computing flows at some combinations of Re and $Q_b : Q_a$ after the idealized geometry had been modified by (i) incorporating a second branch to form an unstaggered or a staggered pair of branches, (ii) rounding the corners of the junction, (iii) introducing a curved aortic wall, or (iv) incorporating a realistically curved inflow tract, flow divider and daughter vessel. None of these modifications had a significant effect on the fundamental flow features or pattern of WSS. Additional evidence for this is provided in figure 5*b*, which shows that similar patterns of streamlines occur along the mid-plane of the aortic channel in the simplified and the more geometrically realistic model of a single branch. It therefore seems unlikely that the use of a real geometry would have altered the main conclusions.

The model was additionally simplified by assuming Newtonian rheology. This assumption is widely used and has only modest quantitative effects on patterns of WSS at branches of large arteries; qualitative features of the pattern and of the fundamental flow are not affected (Perktold *et al.* 1991). Secondary flows emerging from the left ventricle or arising from the curvature and branches of the aortic arch were also ignored; they will have only a minor effect in the descending aorta, most likely by slightly skewing the branch-dependent effects.

The most important simplification was the assumption of steady flow. Some effects of unsteadiness are not considered significant. First, owing to the long wavelength of pressure waves within the aorta (5–10 m; Milnor 1979) and the small deformation of the aortic wall over each cardiac cycle (less than 10% change of aortic diameter), the velocity of radial wall motion is small compared with the radial flow components caused by the branch, and can be ignored. (This may be particularly true for intercostal branch points since they are situated in the dorsal thoracic aorta, which is tethered to the posterior chest wall.) Second, changes in mean velocity during the cardiac cycle are sufficiently slow that the flow can be considered quasi-steady at each time point. This is best understood by using the Strouhal number, St, or its reciprocal, the reduced velocity parameter, U_{red} (Sherwin & Blackburn 2005)

$$U_{red} = \frac{UT}{D_a},$$

where U is the velocity scale and T is the pulse duration. Reduced velocity can be interpreted as the distance (in diameters) that the mean flow covers within one pulse. It is related to the Womersley number, α, and Re according to

$$U_{red} = \frac{\pi Re}{2\alpha^2}.$$

For people ($Re \approx 1500$, $\alpha \approx 15$) and rabbits ($Re \approx 500$, $\alpha \approx 8$), U_{red} is equivalent to approximately 10 aortic diameters, or approximately 100 intercostal branch diameters. Hence, flow near the branch is not dominated by unsteady phenomena and its character can be approximated by the steady flow result obtained at a value of Re appropriate for each part of the cardiac cycle.

However, some effects of unsteadiness could be significant. For example, the inlet velocities should be spatially distributed with a time-varying Womersley profile rather than the Poiseuille profile appropriate for fully developed steady flow. The different distributions of inertia would affect the origin of the streamtube flowing into the branch. We therefore conducted a preliminary investigation of unsteady flow in the simple model geometry of figure 1*a*. A Womersley-type solution for two-dimensional flow driven between two

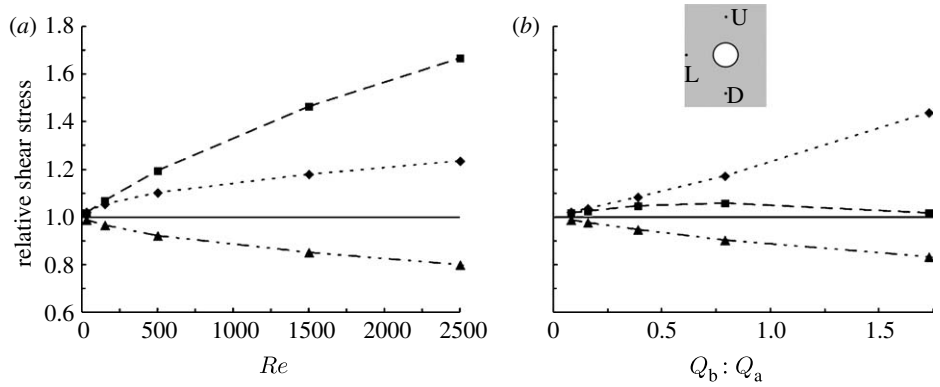

Figure 7. Change in WSS_n with (*a*) Re (for $Q_b : Q_a = 0.08\%$) and (*b*) flow partition (for $Re = 30$), measured at three locations on the aortic wall for the simple geometry of figure 1*a*: at distances 1*D* upstream (U) of the ostial lip, 1*D* downstream (D) of it and 1*D* lateral (L) to it (inset). Dotted line with diamond, U; dashed line with square, D; dot-dashed line with triangle, L.

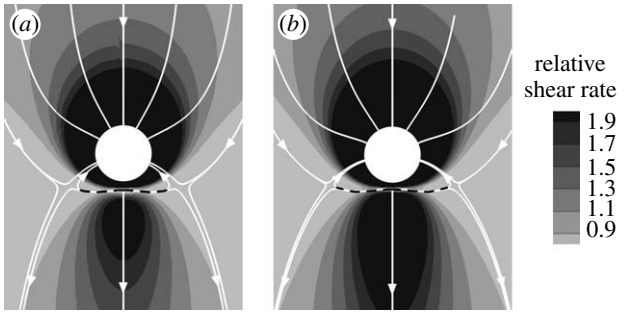

Figure 8. (*a*) Steady flow WSS_n pattern for $Re = 500$, $Q_b : Q_a = 0.79\%$. (*b*) Normalized time-averaged wall shear stress (WSS_n) pattern under unsteady flow conditions, for $Re_m = 500$, $Q_b : Q_a = 0.79\%$ and $U_{red} = 4$ (equivalent to $St = 0.25$). Mean aortic flow is from top to bottom. Dashed lines indicate flow attachment.

parallel plates by a pulsating pressure gradient (Landau & Lifshitz 1959; Loudon & Tordesillas 1998) was applied as inlet velocity profile. The temporal waveform of the sectionally averaged inflow was described by a steady component plus a single sinusoidal harmonic giving a peak-to-mean flow ratio of approximately 1.5. Mean Re was taken to be 500 and U_{red} was 4 (equivalent to $St = 0.25$). A similar waveform, in phase with the aortic inflow waveform and again with a peak-to-mean ratio of 1.5, was imposed on the branch outflow. Mean $Q_b : Q_a$ was 0.79 per cent. Figure 8 compares the pattern of time-averaged WSS_n under these conditions with the steady-flow WSS_n pattern for the same Re and $Q_b : Q_a$ (also shown as figure 2*o*). The two WSS_n patterns are very similar in character, with only slightly more extended regions of high WSS_n upstream and downstream of the branch in the unsteady case; the streamline patterns are indistinguishable.

This preliminary investigation demonstrated that, despite alterations in the pattern of WSS during the cardiac cycle, *mean* WSS_n patterns are not significantly affected by the assumption of steady flow, at least for $U_{red} = 4$ (physically interpreted as the mean flow moving 40 intercostal diameters during one cardiac cycle, and equivalent to a Womersley parameter value of 14). These values represent an upper bound of unsteadiness for the species and ages considered here.

Of course, endothelial cells may respond not only to mean WSS but also to derivatives of WSS and further investigation of the effect of Re and $Q_b : Q_a$ on spatial patterns of such derivatives is required. Several parameters of potential importance have been proposed, including the oscillatory shear index (OSI) and WSS (spatial) gradient (Buchanan *et al.* 1999).

4.2. Comparison with other studies

A number of authors, in seeking to explain the particularly frequent occurrence of lesions downstream of aortic side branches in cholesterol-fed animals (Fry 1969; Cornhill & Roach 1976), or the low frequency of human atherosclerosis at these locations (Caro *et al.* 1971), have speculated that this is an area of particularly high WSS. However, Sobey (1977*a*,*b*) and Tutty (1988), under the assumption of Stokes flow, showed for the two- and three-dimensional case, respectively, that WSS is elevated upstream of small branch orifices as well as downstream of them. Our results are in good agreement with their analyses at similar values of Re and $Q_b : Q_a$ but at other values we found different patterns, involving the occurrence of relatively low WSS at the sides of branches when Re is elevated and downstream of branches when $Q_b : Q_a$ is elevated.

WSS has also been computed in models of the origin of the coeliac artery (Cheer *et al.* 1998; Buchanan *et al.* 1999). This branch is not strictly analogous to the one studied here, since the daughter vessel is comparable in size to the aorta (with a flow partition approaching 50%) and does not form part of a pair. Furthermore, although effects of Re and $Q_b : Q_a$ have been investigated individually (Cheer *et al.* 1998), their interactions have not been studied. Nevertheless, a number of the features and trends we identified can be discerned in the maps they present for this site.

4.3. Physiological and pathological relevance

This study is part of a larger research programme to determine whether the differences in lesion distribution that occur between species and between ages within a species can be explained by differences in the pattern of WSS. Evidence for age- and species-related differences in WSS patterns has been obtained by examining

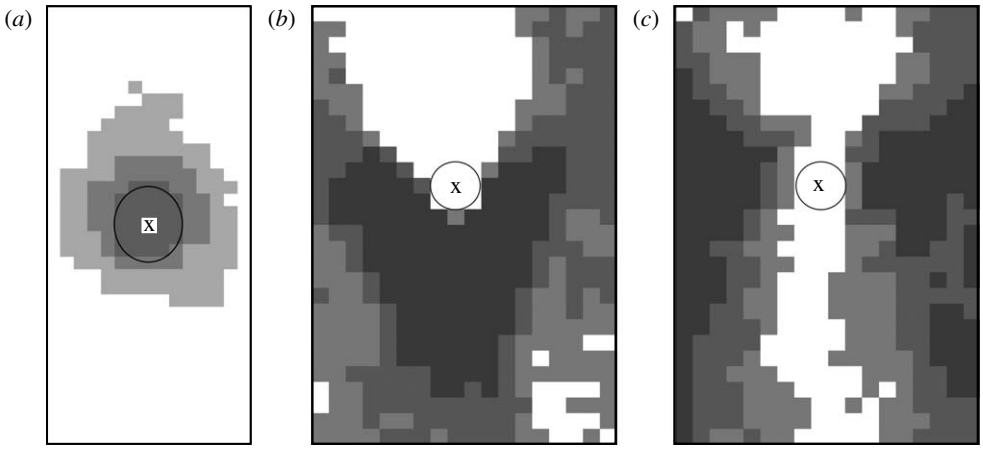

Figure 9. Patterns of lesion frequency around intercostal ostia (*a*) from six mice aged 16–20 weeks (after McGillicuddy *et al.* 2001), (*b*) from six young rabbits, six weeks old, and (*c*) from five mature rabbits of average age 27 months (after Barnes & Weinberg 1999). Frequency increases with shading. Mean aortic flow is from top to bottom and X marks the centre of the ostium.

endothelial morphology around branches. Endothelial cells and their nuclei align with the predominant flow direction and elongate with increasing shear. In young rabbits, endothelial nuclei are more elongated downstream of branches than upstream, but the reverse pattern is seen in mature rabbits (Al-Musawi *et al.* 2004). Nuclear shape is approximately the same upstream and downstream of branches in both immature and mature mice (Bond & Weinberg 2006).

Figure 9*a–c* shows the patterns of aortic lesion frequency around intercostal ostia in apolipoprotein E/low-density lipoprotein receptor double knockout mice (McGillicuddy *et al.* 2001), immature cholesterol-fed rabbits and mature cholesterol-fed rabbits (Barnes & Weinberg 1999), respectively. The comparatively uniform pattern of WSS_n we found for the lowest values of Re and $Q_b : Q_a$ (figure 2*a*) correlates with the approximate circumferential uniformity of lesion frequency seen in mice of all ages (figure 9*a*). Similarly, the WSS_n pattern found at relatively high values of Reynolds and flow rate partition (e.g. for $Re=500$, $Q_b : Q_a=0.79$ per cent in figure 2) correlates with some features of the lesion pattern observed in mature rabbits (figure 9*c*). In both cases, however, other features do not correlate, and we failed to find a pattern of WSS_n that correlates even superficially with the downstream pattern of lesions seen in immature rabbits (figure 9*b*). Despite an apparent consensus, this work showed that many aspects of the relation between WSS and lesion occurrence remain obscure. An examination of spatial and temporal derivatives of WSS under pulsatile flow may help resolve these difficulties.

This work was funded by the Institute of Biomedical Engineering, Imperial College London, and the Public Benefit Foundation Alexander S. Onassis. S.J.S. would also like to acknowledge partial support through an EPSRC Advanced Research Fellowship.

REFERENCES

Abrahams, P. H. 2001 *McMinn's interactive clinical anatomy.* London, UK: Mosby.

Al-Musawi, S. L., Bishton, J., Dean, J., Williams, S., Cremers, S. G. & Weinberg, P. D. 2004 Evidence for a reversal with age in the pattern of near-wall blood flow around aortic branches. *Atherosclerosis* **172**, 79–84. (doi:10.1016/j.atherosclerosis.2003.09.028)

Barnes, S. E. & Weinberg, P. D. 1998 Contrasting patterns of spontaneous aortic disease in young and old rabbits. *Arterioscler. Thromb. Vasc. Biol.* **18**, 300–308.

Barnes, S. E. & Weinberg, P. D. 1999 Two patterns of lipid deposition in the cholesterol-fed rabbit. *Arterioscler. Thromb. Vasc. Biol.* **19**, 2376–2386.

Bond, A. R. & Weinberg, P. D. 2006 Haemodynamic stresses and wall structure can account for the pattern of lipid deposition around aortic branches in mice. *Atherosclerosis* **7**(Suppl.), 200. (doi:10.1016/S1567-5688(06)80777-4)

Buchanan Jr, J. R., Kleinstreuer, C., Truskey, G. A. & Lei, M. 1999 Relation between non-uniform hemodynamics and sites of altered permeability and lesion growth at the rabbit aorto-celiac junction. *Atherosclerosis* **143**, 27–40. (doi:10.1016/S0021-9150(98)00264-0)

Caro, C. G., Fitz-Gerald, J. M. & Schroter, R. 1971 Atheroma and arterial wall shear observation, correlation and proposal of a shear dependent mass transfer mechanism for atherogenesis. *Proc. R. Soc. Lond. B* **177**, 109–159. (doi:10.1098/rspb.1971.0019)

Caro, C. G., Pedley, T. J., Schroter, R. C. & Seed, W. A. 1978 *The mechanics of the circulation.* Oxford, UK: Oxford University Press.

Cheer, A. Y., Dwyer, H. A., Barakat, A. I., Sy, E. & Bice, M. 1998 Computational study of the effect of geometric and flow parameters on the steady flow field at the rabbit aorto-celiac bifurcation. *Biorheology* **35**, 415–435. (doi:10.1016/S0006-355X(99)80020-1)

Cheng, C. *et al.* 2007 Large variations in absolute wall shear stress levels within one species and between species. *Atherosclerosis* **195**, 225–235. (doi:10.1016/j.atherosclerosis.2006.11.019)

Coppola, G., Sherwin, S. J. & Peiró, J. 2001 Nonlinear particle tracking for high-order elements. *J. Comput. Phys.* **172**, 356–386. (doi:10.1006/jcph.2001.6829)

Cornhill, J. F. & Roach, M. R. 1976 A quantitative study of the localization of atherosclerotic lesions in the rabbit aorta. *Atherosclerosis* **23**, 489–501. (doi:10.1016/0021-9150(76)90009-5)

Feintuch, A. *et al.* 2007 Hemodynamics in the mouse aortic arch as assessed by MRI, ultrasound, and numerical modeling. *Am. J. Physiol. Heart Circ. Physiol.* **292**, H884–H892. (doi:10.1152/ajpheart.00796.2006)

Fry, D. L. 1969 Certain chemorheologic considerations regarding the blood vascular interface with particular reference to coronary artery disease. *Circulation* **40**, 38–57.

Giordana, S., Sherwin, S. J., Peiró, J., Doorly, D. J., Crane, J. S., Lee, K. E., Cheshire, N. J. & Caro, C. G. 2005 Local and global geometric influence on steady flow in distal anastomoses of peripheral by-pass grafts. *J. Biomech. Eng.* **127**, 1087–1098. (doi:10.1115/1.2073507)

Greve, J. M., Les, A. S., Tang, B. T., Draney Blomme, M. T., Wilson, N. M., Dalman, R. L., Pelc, N. J. & Taylor, C. A. 2006 Allometric scaling of wall shear stress from mice to humans: quantification using cine phase-contrast MRI and computational fluid dynamics. *Am. J. Physiol. Heart Circ. Physiol.* **291**, H1700–H1708. (doi:10.1152/ajpheart.00274.2006)

Karniadakis, G. & Sherwin, S. J. 2005 *Spectral/hp element methods for computational fluid dynamics*, 2nd edn. Oxford, UK: Oxford Science Publications.

Landau, L. D. & Lifshitz, E. M. 1959 *Fluid mechanics*. Oxford, UK: Pergamon Press.

Loudon, C. & Tordesillas, A. 1998 The use of the dimensionless Womersley number to characterize the unsteady nature of internal flow. *J. Theor. Biol.* **191**, 63–78. (doi:10.1006/jtbi.1997.0564)

McGillicuddy, C. J., Carrier, M. J. & Weinberg, P. D. 2001 Distribution of lipid deposits around aortic branches of mice lacking LDL receptors and apolipoprotein E. *Arterioscler. Thromb. Vasc. Biol.* **21**, 1220–1225. (doi:10.1161/hq0701.091996)

Milnor, W. R. 1979 Aortic wavelength as a determinant of the relation between heart rate and body size in mammals. *Am. J. Physiol. Regul. Integr. Comp. Physiol.* **237**, R3–R6.

Mitchell, J. R. A. & Schwartz, C. J. 1965 *Arterial disease*. Oxford, UK: Blackwell.

Nichols, W. W. & O'Rourke, M. F. 1998 *McDonald's blood flow in arteries. Theoretical, experimental and clinical principles*, 4th edn. London, UK: Arnold.

Papaharilaou, Y., Doorly, D. J. & Sherwin, S. J. 2002 The influence of out-of-plane geometry on pulsatile flow within a distal end-to-side anastomosis. *J. Biomech.* **35**, 1225–1239. (doi:10.1016/S0021-9290(02)00072-6)

Pedley, T. J. 1980 *The fluid mechanics of large blood vessels*. Cambridge, UK: Cambridge University Press.

Peiró, J., Giordana, S., Griffith, C. & Sherwin, S. J. 2002 High-order algorithms for vascular flow modelling. *Int. J. Numer. Meth. Fluids* **40**, 137–151. (doi:10.1002/fld.270)

Perktold, K., Resch, M. & Florian, H. 1991 Pulsatile non-Newtonian flow characteristics in a three-dimensional human carotid bifurcation model. *J. Biomech. Eng.* **113**, 464–475. (doi:10.1115/1.2895428)

Sebkhi, A. & Weinberg, P. D. 1994 Age-related variations in transport properties of the rabbit arterial wall near branches. *Atherosclerosis* **106**, 1–8. (doi:10.1016/0021-9150(94)90077-9)

Sebkhi, A. & Weinberg, P. D. 1996 Effect of age on the pattern of short-term albumin uptake by the rabbit aortic wall near intercostal branch ostia. *Arterioscler. Thromb. Vasc. Biol.* **16**, 317–327.

Shahcheraghi, N., Dwyer, H. A., Cheer, A. Y., Barakat, A. I. & Rutaganira, T. 2002 Unsteady and three-dimensional simulation of blood flow in the human aortic arch. *J. Biomech. Eng.* **124**, 378–387. (doi:10.1115/1.1487357)

Sherwin, S. J. & Blackburn, H. M. 2005 Three-dimensional instabilities and transition of steady and pulsatile axisymmetric stenotic flows. *J. Fluid Mech.* **533**, 297–327. (doi:10.1017/S0022112005004271)

Sherwin, S. J. & Peiró, J. 2002 Mesh generation in curvilinear domains using high-order elements. *Int. J. Numer. Meth. Eng.* **53**, 207–223. (doi:10.1002/nme.397)

Sherwin, S. J., Shah, O., Doorly, D. J., Peiró, J., Papaharilaou, Y., Watkins, N., Caro, C. G. & Dumoulin, C. L. 2000 The influence of out-of-plane geometry on the flow within a distal end-to-side anastomosis. *J. Biomech. Eng.* **122**, 86–95. (doi:10.1115/1.429630)

Sinzinger, H., Silberbauer, K. & Auerswald, W. 1980 Quantitative investigation of sudanophilic lesions around the aortic ostia of human fetuses, newborn and children. *Blood Vessels* **17**, 44–52.

Sloop, G., Perret, R., Brahney, J. & Oalmann, M. 1998 A description of two morphologic patterns of aortic fatty streaks, and a hypothesis of their pathogenesis. *Atherosclerosis* **141**, 153–160. (doi:10.1016/S0021-9150(98)00167-1)

Sobey, I. J. 1977*a* Bio-fluid dynamics of bifurcations. PhD thesis, University of Cambridge, Cambridge, UK.

Sobey, I. J. 1977*b* Laminar boundary-layer flow past a two-dimensional slot. *J. Fluid Mech.* **83**, 33–47. (doi:10.1017/S0022112077001025)

Tutty, O. R. 1988 Flow in a tube with a small side branch. *J. Fluid Mech.* **191**, 79–109. (doi:10.1017/S0022112088001521)

Weinberg, P. D. 2002 Disease patterns at arterial branches and their relation to flow. *Biorheology* **39**, 533–537.

Weinberg, P. D. & Ethier, C. R. 2007 Twenty-fold difference in hemodynamic wall shear stress between murine and human aortas. *J. Biomech.* **40**, 1594–1598. (doi:10.1016/j.jbiomech.2006.07.020)